Comprehensive Analysis of the Effects of CdSe Quantum Dot Size, Surface Charge, and Functionalization on Primary Human Lung Cells

Amber Nagy,[†] Andrea Steinbrück,[‡] Jun Gao,[†] Norman Doggett,[†] Jennifer A. Hollingsworth,[‡] and Rashi Iyer[†,*]

[†]Biosecurity and Public Health, Bioscience Division, and [‡]Center for Integrated Nanotechnologies, Materials Physics & Applications Division, Los Alamos National Laboratory, Los Alamos, New Mexico 87545, United States

ABSTRACT The growing potential of quantum dots (QDs) in applications as diverse as biomedicine and energy has provoked much dialogue about their conceivable impact on human health and the environment at large. Consequently, there has been an urgent need to understand their interaction with biological systems. Parameters such as size, composition, surface charge, and functionalization can be modified in ways to either enhance biocompatibility or reduce their deleterious effects. In the current study, we simultaneously compared the impact of size, charge, and functionalization alone or in combination on biological responses using primary normal human bronchial epithelial cells. Using a suite of cellular end points and gene expression analysis, we determined the biological impact of each of these properties. Our results suggest that positively charged QDs are significantly more cytotoxic compared to negative QDs. Furthermore, while QDs functionalized with long ligands were found to be more cytotoxic than those functionalized with short ligands, negative QDs functionalized with long ligands also demonstrated size-dependent cytotoxicity. We conclude that QD-elicited cytotoxicity is not a function of a single property but a combination of factors. The mechanism of toxicity was found to be independent of reactive oxygen species formation, as cellular viability could not be rescued in the presence of the antioxidant *n*-acetyl cysteine. Further exploring these responses at the molecular level, we found that the relatively benign negative QDs increased gene expression of proinflammatory cytokines and those associated with DNA damage, while the highly toxic positive QDs induced changes in genes associated with mitochondrial function. In an attempt to tentatively "rank" the contribution of each property in the observed QD-induced responses, we concluded that QD charge and ligand length, and to a lesser extent, size, are key factors that should be considered when engineering nanomaterials with minimal bioimpact (charge > functionalization > size).

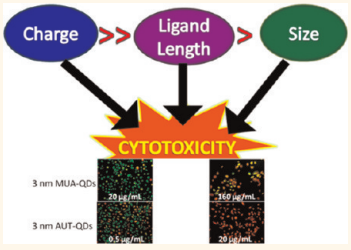

KEYWORDS: quantum dots · bronchial epithelial cells · cytotoxicity · reactive oxygen species · mitochondrial function

Quantum dots (QDs) are semiconductor nanocrystals that possess unique properties including highly efficient photoluminescence that can be "color" tuned by simple modification of QD size, permitting complex multiplexing schemes. In addition, compared to traditional organic fluorophores, QDs are resistant to photobleaching, and they can be heterostructured to suppress or eliminate fluorescence intermittency (blinking).[1−4] QDs are becoming prominent in the biomedical field for applications such as disease diagnostics,[5−8] cellular and molecular tracking,[9−14] end-point assay measurements,[15−17] small animal imaging,[18−20] and therapeutic drug delivery.[21,22] They are also being investigated for a range of applications outside of biology and nanomedicine, including light-harvesting agents in next-generation photovoltaics and as active light emitters in solid-state lighting. Although their potential for affecting a significant and broad technological impact is relatively well studied and understood, their potential to generate unexpected consequences with respect to human health and the environment is less well appreciated. As a result of their nanoscale size and, in the case of heavy-metal-comprising QDs, their chemical composition, physicochemical factors such as size, core composition, surface chemistry, and redox properties may influence QD−biological interactions individually or collectively, thereby necessitating a multimodal approach to evaluating QD toxicity. Given their envisioned applications, QDs will likely be either directly and intentionally exposed to biological systems or inadvertently introduced during scaled-up production, transport, and end-use applications. In anticipation of this progression from basic research to commercial products, comprehensive bioresponse assessments are required that address the full complexity of these important nanomaterials.

Previous studies investigating the toxicity of QDs have tended to focus on QD core composition,[23] size, or surface functionality,

* Address correspondence to rashi@lanl.gov.

Received for review December 13, 2011 and accepted May 15, 2012.

Published online May 15, 2012
10.1021/nn204886b

and indeed, these palpable features have been shown to influence cytotoxicity. For example, Li *et al.* found that ZnS QDs were less cytotoxic than CdSe QDs of the same size and surface functionalization,[24] demonstrating that a cadmium-derived toxic response could be reduced by encapsulating the Cd-containing QD core within a shell. This was further supported by Cho *et al.*, who showed that CdSe/ZnS core/shell QDs were less toxic compared to CdTe QDs.[23] Similarly, Wang *et al.* used Caco-2 cells to show that CdTe QDs coated with surfactant were more toxic than CdTe/ZnS core/shell QDs capped with polyethylene glycol (PEG).[25] With respect to size effects, Lovrić *et al.* observed that the subcellular distribution and toxicity of CdTe QDs change dramatically as a function of QD size.[26] Other studies have shown that QD surface charge can affect cytotoxicity,[27] with positive QDs being more toxic than negative QDs.[28] Additional aspects of surface functionalization can dictate QD-derived cytotoxicity, as well.[29,30] While each of these studies have provided useful information on the impact of a specific QD property (composition, size, or surface functionalization), a comparative analysis is needed to determine the degree to which each of these properties, in isolation or in combination, affect cellular responses. Although it is evident that QDs elicit cellular and molecular level responses, it is still unclear as to what specific properties drive the observed QD-induced biological responses.

To address this gap, we have performed a comprehensive and systematic analysis to understand the effect of relevant QD properties: size, surface charge, and functionalization, keeping the QD core composition constant (CdSe), on key cellular responses. Because QDs are used for a wide range of applications, QDs were prepared in the absence of a shell to better understand how factors such as charge and functionalization modulate cellular response. Accordingly, we utilized QDs that are 3, 5, or 10 nm in size, functionalized to have either a negative surface charge using mercaptoundecanoic acid (MUA) or mercaptopropanoic acid (MPA) or a positive surface charge using amino undecanethiol (AUT) or cysteamine (CYST). Both MUA and AUT are characterized by relatively more steric bulk compared to MPA or CYST, where the former ligands possess alkane chain lengths comprising 11 carbon atoms, compared to the latters' 3 and 2 carbon atoms, respectively. Although QD cytotoxicity has previously been investigated *in vitro* using a wide range of cell types, including murine macrophages, human epidermal keratinocytes, rat hippocampal neurons, and bovine corneal stromal cells,[31−34] we used primary human pulmonary epithelial (NHBE) cells to represent exposure *via* inhalation. As applications for QDs continue to grow, inhalation becomes a key potential route of exposure since QDs can exist in aerosolizable liquid forms or even as dispersible powders, due to their nanoscale size and surface functionalization.

More specifically, we assessed the properties-dependent response of primary human bronchial epithelial cells using a suite of CdSe QDs. We evaluated the effect of each of these materials on cellular cytotoxicity, metabolism, proliferation, and redox status. Our results indicated a size dependency in the magnitude of response elicited, positively charged QDs more impactful than negatively charged QDs, and QDs functionalized with longer-chain ligands more detrimental to cell function than those coated with shorter-chain ligands. Toward a better understanding of the role of ROS in QD-mediated effects, we investigated QD-generated ROS response in the absence and presence of the antioxidant *n*-acetyl cysteine (NAC), and cellular viability was not rescued by NAC, suggesting minimal if any role for ROS in the observed cytotoxicity. To further understand the mechanistic underpinnings of the observed responses as a function of nanomaterial property, we monitored changes in gene expression levels.

RESULTS

QD Characterization. In an attempt to clarify the individual and/or collective roles played by various QD physicochemical properties, we investigated a range of CdSe QD sizes, charges, and surface chemistries. Specifically, we synthesized 3, 5, and 10 nm diameter CdSe QDs (characterized spectrally using UV−vis absorption spectroscopy and structurally by TEM, Figure 1) and rendered them positively or negatively charged using either short (MPA, CYST) or long-chain (MUA, AUT) ligands. All ligands contained a thiol moiety that facilitated binding to the QD surfaces. MPA and MUA terminated in carboxyl groups, which afforded negatively charged QDs, while CYST and AUT terminated in amine groups, which afforded positively charged QDs. QD hydrodynamic diameter and stability were determined by dynamic light scattering (DLS) and zeta-potential analysis (Table 1), respectively. As all QD systems in this study were stabilized exclusively by electrostatic stabilization, that is, by way of surface charge rather than addition of hydrophilic moieties such as polyethyleneglycol (PEG) segments, zeta-potential is a key measure of aqueous-phase particle stability. Zeta-potential values of greater than ±30 mV are generally considered sufficiently large to afford long-term stability.[35] Here, only the MUA-stabilized 10 nm QDs failed to reach this value. DLS results revealed that the QDs in water either did not aggregate (*e.g.*, MPA-, MUA-, and CYST-stabilized 3 nm QDs) or did form small aggregates (*e.g.*, CYST-stabilized 5 and 10 nm QDs). AUT-stabilized QDs of all sizes showed the greatest tendency toward aggregation, though even in these cases the QDs did not visibly fall out of solution, and the mixtures retained optical clarity. Subsequent DLS measurements of solutions

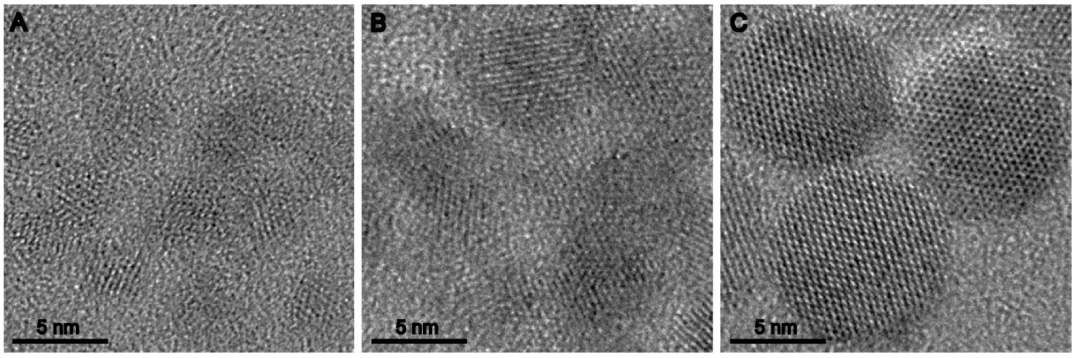

Figure 1. High-resolution TEM images of 3 nm (A), 5 nm (B), and 10 nm (C) CdSe QDs.

TABLE 1. CdSe QD Physicochemical Properties

physical diameter [nm] (from TEM)	ligand	hydrodynamic diameter from DLS [nm] (derived from the number distribution)	zeta-potential [mV]
3 nm	MUA	5.11 ± 1.26	−71.8 ± 11.5
(3.37 ± 0.57)	MPA	4.69 ± 1.03	−56.0 ± 10.9
	AUT	9.70 ± 1.34	86.8 ± 9.83
	CYST	3.68 ± 1.14	57.4 ± 16.2
5 nm	MUA	7.56 ± 0.90	−53.5 ± 10.6
(4.98 ± 0.80 nm)	MPA	15.7 ± 5.49	−29.4 ± 5.62
	AUT	122.8 ± 9.10	73.7 ± 17.4
	CYST	15.2 ± 3.10	43.4 ± 0.89
10 nm	MUA	46.4 ± 9.04	−21.0 ± 5.16
(9.48 ± 1.26 nm)	MPA	59.5 ± 22.5	−39.0 ± 4.98
	AUT	90.6 ± 15.1	60.6 ± 15.5
	CYST	42.6 ± 15.9	46.7 ± 6.28

of electrostatically stabilized QDs stored in the dark and cold demonstrated that these solutions were stable to further aggregation from weeks (AUT-QDs) to months (all others).

Preliminary experiments were performed to determine a range of concentrations for subsequent exposure. No significant cytotoxicity was observed for the negatively charged QDs at the lower concnetrations from 0.5 to 20 μg/mL, while the positively charged QDs showed significant cytotoxicity even at 0.5 μg/mL. All subsequent experiments were performed using a concentration range straddling "no observable effects" to "significant observable effects". Therefore, normal primary human bronchioepithelial cells were exposed to the different CdSe QDs at concentrations of 20, 80, or 160 μg/mL for the negatively charged QDs and 0.5, 3.5, 5, or 20 μg/mL for the positively charged QDs. The considerable disparity in the dose response between the positive and negative QDs was not entirely unexpected. We posit that the observed charge-dependent differences might be due to the propensity of positively charged QDs to interact with the negatively charged cell membrane.

Surface Charge and Capping Ligand Determine Nature and Degree of Cytotoxicity. To quantify the effect of QD surface charge on cellular viability, we assessed the apoptotic and necrotic potential of the QDs. Apoptosis is programmed cell death, where cellular metabolic activity is shut down in response to either extracellular or intrinsic triggers, while necrosis is premature cell death caused by external stimuli, such as a toxin or infection. Necrosis was evaluated by measuring the release of lactate dehydrogenase (LDH) 24 h after exposure. As expected, on the basis of our initial dose-dependent exposure studies, positively charged QDs were found to be highly necrotic at much lower concentrations compared to negatively charged QDs (3.5 μg/mL compared to 80 μg/mL, respectively). This charge-induced necrotic trend was observed irrespective of ligand length (Figure 2). While AUT-QDs (long, positively charged ligands) were toxic at all concentrations tested, CYST-QD (short, positively charged ligands) caused necrosis only at the higher concentration and did not induce cell damage at the lower concentrations (Supporting Information Supplemental Figure 1). Overall, the positively charged QDs were clearly more damaging than the negatively charged MPA- or MUA-functionalized QDs. Negatively charged, MUA-functionalized QDs were found to induce a size-dependent increase in necrosis compared to MPA-functionalized QDs, which were not found to be at all necrotic. Thus, while negatively charged QDs appear to be notably more benign than the positively charged QDs, it is possible to chose or design positively charged ligands that are sufficiently nontoxic with respect to necrosis at lower concentrations.

Further evidence for charge-based disparity in the induction of cellular cytotoxicity was obtained by comparing QD-induced apoptosis. Fluorescent acridine orange/ethidium bromide staining revealed drastic differences in the number of apoptotic cells after QD treatment. Cells were treated with media, QDs, or the apoptosis-inducing agent, camptothecin, as the positive control. Figure 3A,B shows an increase in apoptotic cells when exposed to positively charged QDs compared to negatively charged QDs. These results were

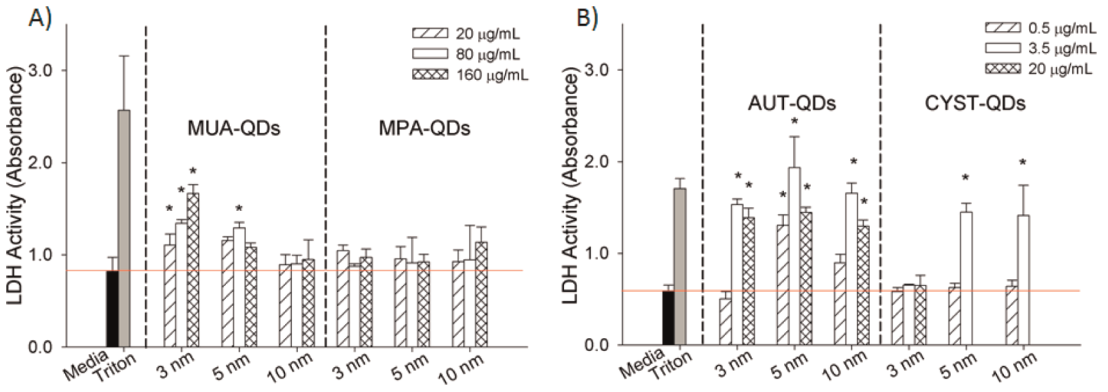

Figure 2. Necrosis of NHBE cells after 24 h exposures to 3, 5, and 10 nm CdSe QDs bearing different charges and functionalization groups. (A) Negatively charged 3, 5, and 10 nm CdSe QDs capped with MUA or MPA were applied to NHBE cells at concentrations of 20, 80, or 160 μg/mL for 24 h, and necrosis was measured by evaluating the activity of lactate dehydrogenase found in cell supernatants. Values are mean $\pm$ standard deviation from three independent experiments. Significant differences compared to the media control are denoted with *, $p < 0.025$. Red line is an aid to denote baseline levels. (B) Positively charged 3, 5, and 10 nm CdSe QDs capped with AUT or CYST were applied to NHBE cells at concentrations ranging from 0.5, 3.5, or 20 μg/mL for 24 h, and necrosis was measured by evaluating the activity of lactate dehydrogenase found in cell supernatants. Values are mean $\pm$ standard deviation from three independent experiments. Significant differences compared to the media control are denoted with *, $p < 0.001$. Red line is a visual aid to denote baseline levels.

confirmed using quantitative histone-based ELISA assays (Figure 3C,D). No significant apoptosis was observed in the MUA-capped negatively charged QDs, with the exception of the 10 nm QD at the highest concentration of 160 μg/mL. Moreover, there was no observable difference between the media control and MPA-QDs. In contrast, the AUT-capped positively charged QDs induced significant apoptosis at the lowest concentration of 0.5 μg/mL. The lack of apoptosis noted at the higher concentrations (3.5 and 20 μg/mL) as observed by the histone ELISA was probably due to the significant necrosis caused at these concentrations, which resulted in a corresponding decrease in observable apoptosis. However, the 3 nm CYST-capped QDs did not induce apoptosis compared to media-treated cells, whereas the 5 and 10 nm QDs caused modest apoptosis at both concentrations.

QD Surface Charge Affects NHBE Proliferation. To determine if charge, ligand, or size impact the proliferative ability of cells, we used water-soluble tetrazolium salt (WST-1) to measure the metabolic activity of exposed cells. The proliferation response of NHBE cells after exposure to positively or negatively charged QDs appeared to result from a combination of ligand charge and length effects. Though similarly charged, 3 nm MPA-QDs and MUA-capped QDs were found to have an opposite proliferative effect. As expected, on the basis of the cell death observations, cellular proliferation after exposure to the 3 and 5 nm MUA negatively charged QDs was significantly decreased when compared to control cells, while proliferation of cells exposed to MPA-capped QDs of all sizes was generally not changed (Figure 4A). The decrease in metabolic activity observed in 3 and 5 nm MUA-capped QDs is likely an artifact of the considerable necrosis induced by these QDs at all three concentrations. Neither 10 nm MUA-QDs nor 10 nm MPA-QDs significantly affected proliferation (*e.g.*, only the highest concentration MPA-QDs, 160 μg/mL, resulted in a decrease in proliferation compared to media controls). These results correlate well with the minimal cell death observed for both. This cause (cell death) and effect (reduced proliferation) response is further reiterated in the AUT-capped positively charged QDs. Cells exposed to 3 or 5 nm QDs containing longer ligands (AUT or MUA) were significantly less proliferative compared with QDs capped with the shorter ligands (Figure 4A, B). One notable exception is that proliferation was unchanged for cells exposed to 10 nm MUA-QDs, while cells exposed to 10 nm AUT-QDs demonstrated attenuated proliferation (Figure 4A,B). Decreased proliferation was noted in cells exposed to 3 nm CYST-QDs, while cells exposed to 5 and 10 nm CYST-QDs, surprisingly, also induced metabolic activity, indicating these QDs might very well trigger a surprising range of cell responses.

QD-Induced Reactive Oxygen Species (ROS) Production. We evaluated the redox status of cells on exposure to the different QDs using the redox-sensitive nonfluorescent dye 5-(and-6)-carboxy-2′,7′-dichlorodihydrofluorescein diacetate, acetyl ester (CM-H_2DCFDA), which fluoresces in response to intracellular ROS. Cells treated with H_2O_2 were used as positive controls, and media-only-treated cells served as the baseline (as indicate by red lines in Figure 5). The negatively charged MUA-QDs and the positively charged AUT-QDs caused significant enhancement in intracellular ROS production compared to H_2O_2-treated cells. In contrast, the MPA-capped negatively charged and the CYST-capped positively charged QDs did not induce significant redox stress in these cells (Figure 5A,B). The lack of ROS

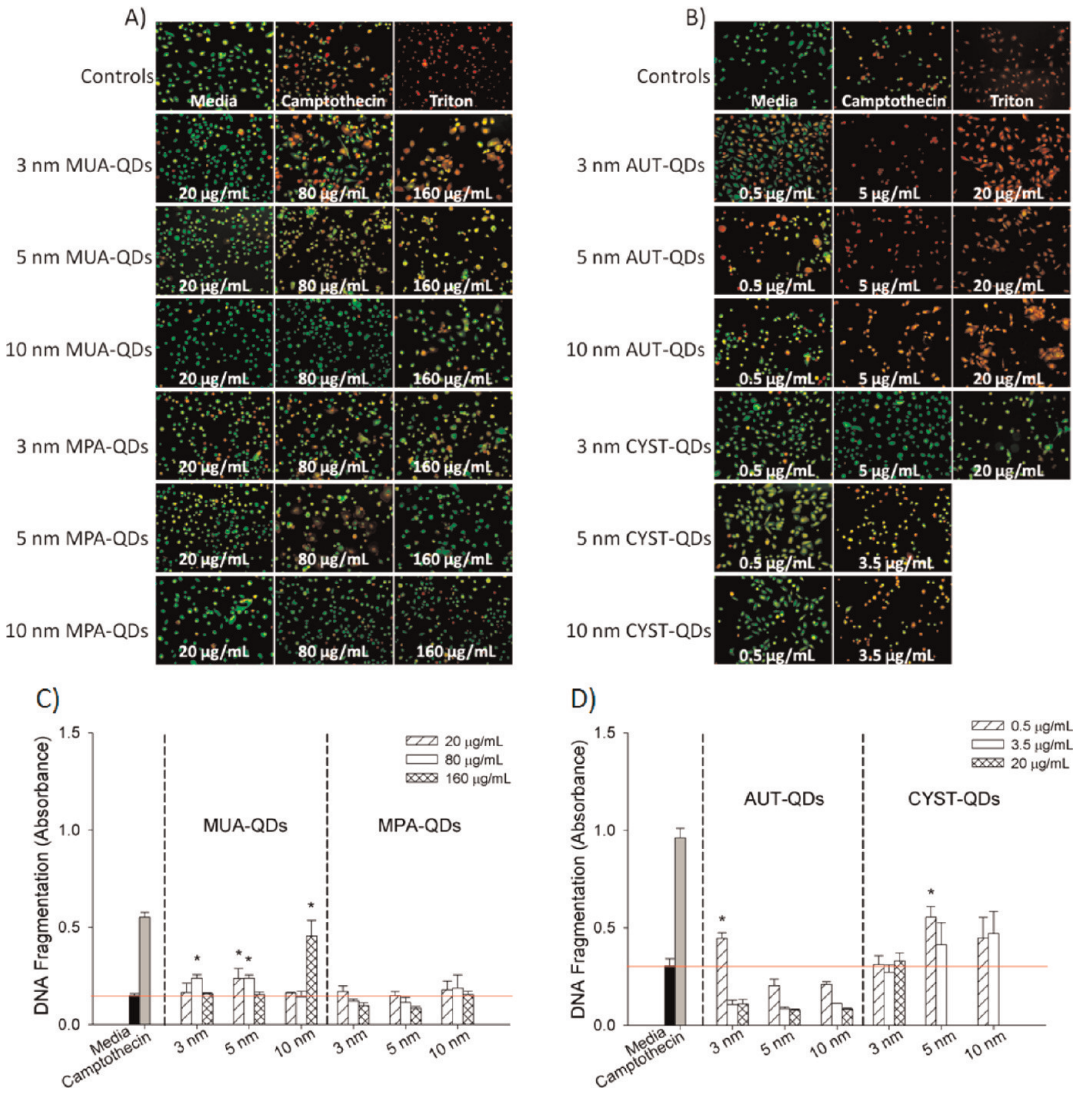

Figure 3. Viability and apoptotic effects of 3, 5, and 10 nm QDs with different charges and surface functionalization groups. (A) NHBE cells were exposed to 20, 80, or 160 μg/mL of 3, 5, and 10 nm MUA-QDs or MPA-QDs for 24 h prior to staining with acridine orange/ethidium bromide. Images are magnified using a 10$\times$ objective and are representative of three independent experiments. (B) NHBE cells were exposed 3, 5, or 10 nm AUT-QDs or CYST-QDs at concentrations of 0.5, 3.5, 5, or 20 μg/mL for 24 h prior to staining with acridine orange/ethidium bromide. Images are magnified using a 10$\times$ objective and are representative of three independent experiments. (C) Cells were exposed to 20, 80, or 160 μg/mL of 3, 5, and 10 nm MUA-QDs or MPA-QDs for 24 h prior to lysis. Sample lysates were analyzed for DNA fragmentation *via* histone ELISA. Values are mean $\pm$ standard deviation from three independent experiments. Significance differences compared to the media control is denoted with *, $p < 0.01$. Red line is a visual aid to denote baseline levels. (D) Cells were exposed to AUT-QDs or CYST-QDs at concentrations of 0.5, 3.5, or 20 μg/mL for 24 h. Cell lysates were analyzed for DNA fragmentation *via* histone ELISA. Values are mean $\pm$ standard deviation from three independent experiments. Significance differences compared to the media control is denoted with *, $p < 0.025$. Red line is a visual aid to denote baseline levels.

response for 3 and 5 nm AUT-QDs at 20 μg/mL could be attributed to the high toxicity of these QDs at these concentrations (Figure 2), as 10 nm AUT-capped QDs caused an increase in ROS levels at similar concentrations.

Previous studies have indicated that treatment with antioxidants can preserve cellular viability. In our study, MUA-QDs and AUT-QDs were found to induce both ROS and cytotoxicity, therefore NHBE cells were pretreated with the antioxidant *n*-acetyl cysteine (NAC) followed by exposure to QDs suspended in media also containing NAC. The formation of ROS was reduced to baseline for all of the cells exposed to QDs + NAC (Figure 5C,D). To determine if antioxidants can protect cells from damage induced by ROS, ATP levels were measured after 24 h exposure to MUA and AUT-QDs in the presence and absence of NAC. ATP levels were decreased in a dose-dependent manner for cells exposed to 3 and 5 nm MUA QDs, while ATP levels for cells exposed to 10 nm MUA-QDs were not affected (Figure 6A). NHBE cells exposed to AUT-QDs for 24 h had reduced levels of ATP compared to media at all concentrations tested (Figure 6B). Surprisingly, ATP levels were not increased when cells were concurrently

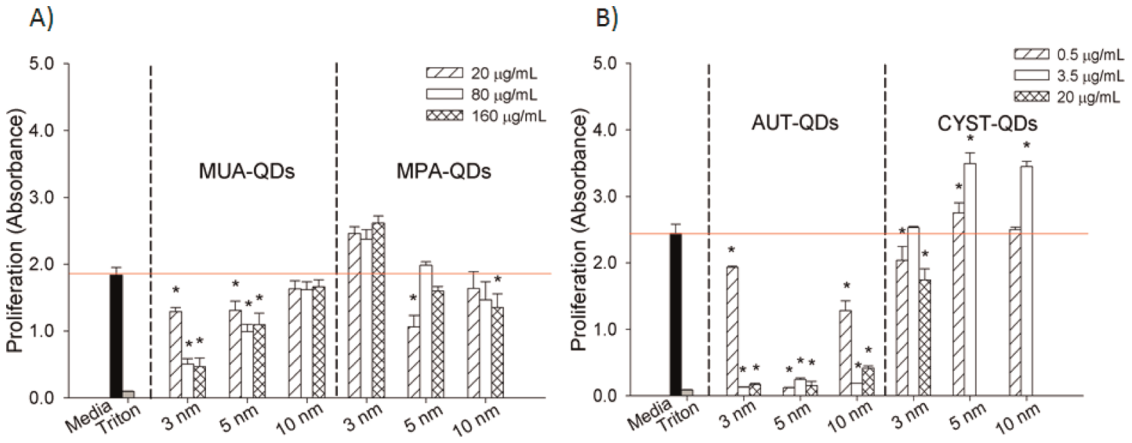

Figure 4. QDs of 3, 5, and 10 nm containing different charge and surface functional groups have a differential impact on NHBE proliferation. (A) NHBE cells were exposed to MUA- or MPA-QDs at concentrations of 20, 80, or 160 μg/mL for 22 h. Values are mean $\pm$ standard deviation and are representative of three independent experiments. Significance compared to media control is delineated by * and $p < 0.05$. Red line is a visual aid to denote baseline levels. (B) NHBE cells were exposed to AUT-QDs or CYST-QDs at concentrations of 0.5, 3.5, or 20 μg/mL for 22 h. Values are mean $\pm$ standard deviation of fold change above media control (indicated by the red line). Significance compared to media control is delineated by *, $p < 0.01$.

exposed to MUA-QDs and AUT-QDs in the presence of NAC (Figure 6A,B). Accordingly, the presence of NAC was not able to preserve cell viability (Figure 6C), although ROS levels were reduced to baseline (Figure 5C,D).

QD-Induced Gene Level Responses. While cell response end-point assays are useful to determine cytotoxicity and changes in cellular metabolism, they provide little insight into the mechanisms driving cell death. Thus, we investigated the up-regulation and down-regulation of genes known to play crucial roles in cellular processes including apoptosis, mitochondrial function, and inflammation using real-time PCR analyses. Comparing gene expression changes between negatively and positively charged 3 nm QDs (constant size, at a concentration of 20 μg/mL), the positively charged QDs up-regulated genes involved with mitochondrial function (CYP1A2 and UCP1), irrespective of ligand (Table 2). Additionally, CASP9, which is involved in apoptosis was also up-regulated in cells exposed to positively charged QDs. Both negative and positive QDs caused increases in gene expression associated with extracellular matrix remodeling (MMP9 and MMP1, respectively). Negative QDs also induced expression of several genes associated with inflammation. Specifically, genes coding for IL-6 and IL-8 were up-regulated ~9.5-fold and ~4.5 fold for cells exposed to 3 nm MUA-QDs. Even though cells exposed to 3 nm MPA-QDs did not induce cytotoxicity, genes coding for IL-6 and IL-8 were up-regulated ~31.5-fold and 3.6-fold, respectively (Table 2).

Because of the massive cytotoxicity induced by positive QDs, we compared gene expression levels in cells exposed to 0.5 μg/mL of AUT-QDs and CYST-QDs. Notable differences in gene expression in response to QDs capped with AUT and CYST (Table 3) were observed. While 3 nm CYST-QDs were relatively noncytotoxic, gene expression associated with mitochondrial function (CYP1A1, CYP1B1, and UCP3) was significantly up-regulated. Interestingly, genes coding for several chemokine ligands (CXCL1, CXCL2, and CXCL3) and chemokine receptors (CCR3 and CCR4) were significantly up-regulated in cells exposed to 3 nm AUT-QDs compared to CYST-QDs. Further, the pro-apoptotic genes (BAD and CASP9) were significantly up-regulated in cells exposed to AUT-QDs, which is consistent with the increase in DNA fragmentation shown in Figure 3B. It also appears that AUT-QDs up-regulate the proto-oncogenes cJUN and cMYC, indicating that complex cellular regulation occurs in response to QD exposure.

DISCUSSION

Conventional "mass-based" approaches are typically used for toxicological studies and are extensively utilized for establishing regulatory standards for molecular compounds, and bulk materials are likely not adequate for establishing similar standards for engineered nanomaterials whose physicochemical properties are not a simple function of composition. While there is a critical need for a systematic evaluation and understanding of NP properties-dependent responses in biosystems, it is also an exceedingly complex and momentous task. Nevertheless, there has been some effort to address this gap and provide tentative guidelines, not only to tackle uncertainties about the toxicity of these novel materials but also to provide design parameters to enable the development of "high-function, low-bioimpact" nanomaterials. Indeed, several studies have attempted to "tease" out the impact of individual chemical and physical nanoparticle properties on humans and the environment. While QDs have the potential to transform the discipline of bioimaging, their potential use for energy harvesting light sources and as photodetectors increases the likelihood of

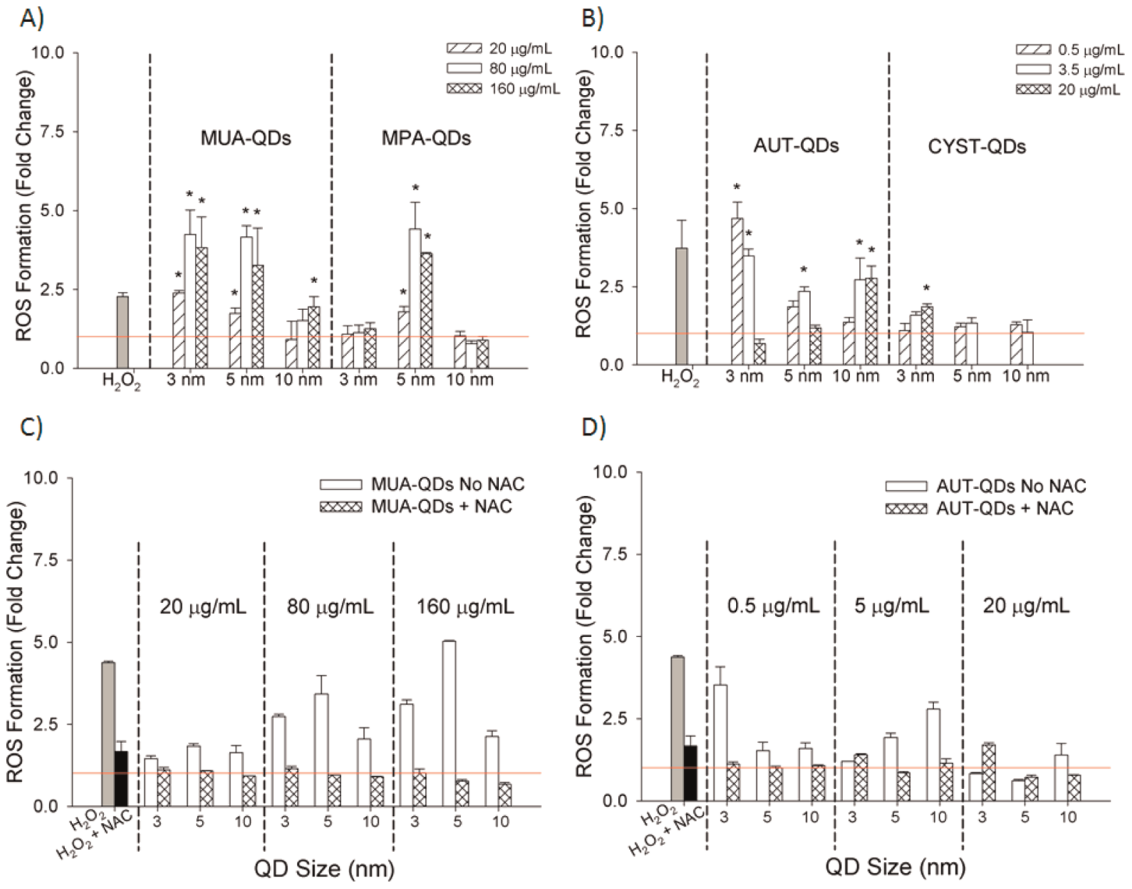

Figure 5. NHBE cells produce intracellular ROS after a 1 h exposure to 3, 5, and 10 nm QDs with different charges and functional groups. Red line is a visual aid to denote baseline levels. (A) NHBE cells were stained with H_2DCFDA for 30 min prior to exposure to MUA-QDs or MPA-QDs at concentrations of 20, 80, or 160 μg/mL. Fluorescence readings were taken at 30, 60, and 90 min. Data graphed are from 60 min readings. Values are mean ± standard deviation of fold change above media control (indicated by the red line). Significance compared to media control is delineated by * and $p < 0.025$. (B) NHBE cells were stained with H_2DCFDA for 30 min prior to exposure to 3, 5, or 10 nm AUT-QDs or CYST-QDs at concentrations of 0.5, 3.5, or 20 μg/mL. Fluorescence readings were taken at 30, 60, and 90 min. Data graphed are from 60 min readings and representative of three independent experiments. Values are mean ± standard deviation of fold change above media control (indicated by the red line). Significance compared to media control is delineated by * and $p < 0.01$. (C) H_2DCFDA stained NHBE cells were pretreated with 5 mM of NAC. Cells were then exposed to increasing concentrations of 3, 5, or 10 nm MUA-QDs. Values are mean ± standard deviation of fold change above media control (indicated by the red line). (D) H_2DCFDA stained NHBE cells were pretreated with 5 mM of NAC. Cells were then exposed to increasing concentrations of 3, 5, or 10 nm AUT-QDs. Values are mean ± standard deviation of fold change above media control (indicated by the red line).

environmental, occupational, and consumer exposure. With regard to QDs, the emphasis has been primarily on composition due to the potential of heavy-metal-induced toxicity caused by the cadmium, selenium, or telluride core. All of these materials have known human toxicity.[36−42] To address this, several synthetic schemes have been developed to "shield" the CdSe or CdTe core by coating with shells, such as ZnS. Moreover, to enhance function and broaden potential applications, core and shell size have been manipulated to change size, semiconductor cores and shells may be "decorated" on the surface with ligands to increase solubility (QDs are inherently hydrophobic), impart charge, and enable targeting. All of these manipulations influence the ability of these nanomaterials to interact with biological molecules and systems. In fact, a number of studies have demonstrated that modifications to the core physical and chemical properties of QDs, such as selection of an appropriate shell coating,[23,43] modulation of surface charge[32] or surface coating,[23] lower dosage of QDs,[33] or optimizing the size of the QDs,[44] can potentially impact their toxicity. Thus, we embarked on this study using CdSe QDs, devoid of shells, but synthesized to independently investigate the effects of QD size, functionalization, and charge. The cellular response results for necrosis, apoptosis, proliferation, and reactive oxygen species have been categorized below in Table 4 to better provide a synopsis of our findings and potential conclusions.

Of the three QD physicochemical properties—core size, ligand length, and surface charge—we find that charge plays a pivotal role in the ability of QDs to induce cellular toxicity. Gross cytotoxicity results, as observed by necrotic and apoptotic cell death, suggest that positively charged CdSe QDs induce severe cell

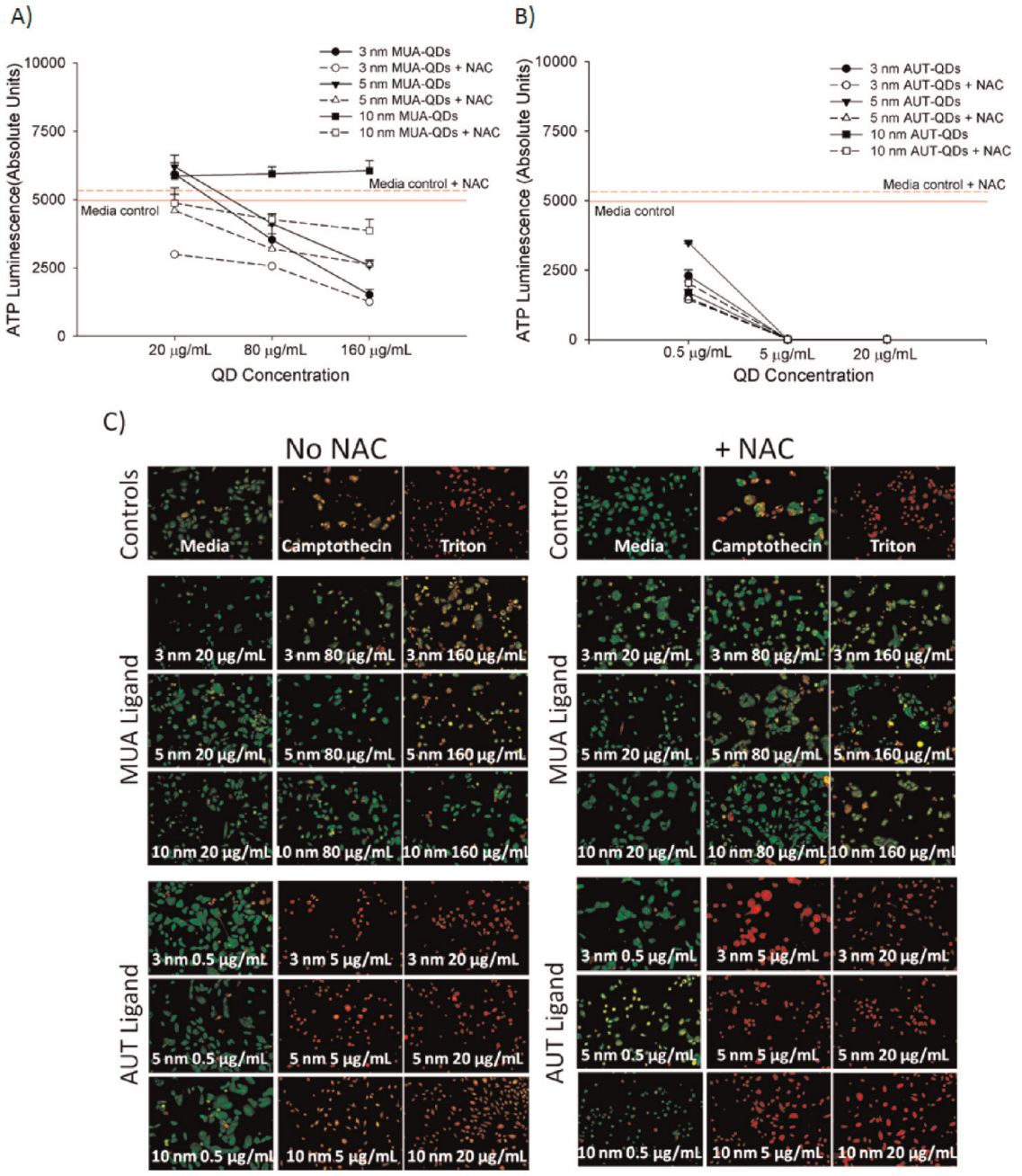

Figure 6. Co-treatment of NHBE cells with 3 nm MUA-QDs or 3 nm AUT-QDs and the antioxidant *n*-acetyl cysteine for 24 h does not rescue cell viability, indicating that the observed cytotoxicity may be ROS-independent. (A) NHBE cells were either exposed to 3, 5, or 10 nm MUA-QDs or AUT-QDs suspended in BEGM in the absence of NAC or pretreated with NAC prior to exposing cells to 3, 5, or 10 nm MUA-QDs for 24 h. Cells were then washed with PBS and lysed. ATP was then quantified by luminescence. (B) NHBE cells were either exposed to 3, 5, or 10 nm MUA-QDs or AUT-QDs suspended in BEGM in the absence of NAC or pretreated with NAC prior to exposing cells to 3, 5, or 10 nm AUT-QDs for 24 h. Cells were then washed with PBS and lysed. ATP was then quantified by luminescence. (C) NHBE cells were either exposed to 3, 5, or 10 nm MUA-QDs or AUT-QDs suspended in BEGM in the absence of NAC or pretreated with NAC prior to exposing cells to 3, 5, or 10 nm MUA-QDs or AUT-QDs for 24 h. Cells were washed with PBS, stained with acridine orange/ethidium bromide and imaged immediately. Images are magnified using a 10× objective and are representative of three independent experiments.

death at concentrations much lower than their negatively charged counterparts. This response was independent of the length of the surface ligand and largely independent of QD core size, as both AUT-capped and CYST-QDs induced cell death irrespective of core size, with the notable exception of the 3 nm positively charged QDs. Positively charged 3 nm CYST-QDs afforded more benign, or at least less variable, results compared to 3 nm AUT-QDs. At lower concentrations (0.5 μg/mL), 3 nm AUT-QDs and all three concentrations of the 3 nm CYST-QDs exhibited no necrotic response compared to control cells. With respect to apoptotic response, the 3 nm AUT-QDs induced little apoptosis, likely due to their ability to initiate overwhelming necrosis in cells, while the 3 nm CYST-QDs

TABLE 2. Differences in Gene Expression for NHBE Cells Exposed to 20 μg/mL of 3 nm QDs for 6 h

		gene expression fold change			
associated pathway	*gene ID*	3 nm MUA-QDs	3 nm MPA-QDs	3 nm AUT-QDs	3 nm CYST-QDs
angiogenesis	*ANGPT1*	0.60 ± 0.24	0.53 ± 0.09	2.43 ± 0.65	3.97 ± 1.19
	ANGPT2	1.53 ± 0.75	3.10 ± 0.80	2.22 ± 0.15	1.12 ± 0.15
apoptosis and DNA damage	*BCL-2*	0.60 ± 0.21	0.53 ± 0.14	2.70 ± 0.13	1.11 ± 0.15
	CASP9	0.43 ± 0.07	0.44 ± 0.08	3.10 ± 0.34	2.03 ± 0.15
	GADD45A	2.41 ± 0.50	2.54 ± 0.26	1.05 ± 0.01	1.75 ± 0.04
cytokines and chemokines	*CCR1*	0.85 ± 0.35	0.68 ± 0.15	1.82 ± 0.26	4.61 ± 1.90
	CCR3	0.51 ± 0.25	0.41 ± 0.25	1.93 ± 0.07	4.15 ± 0.77
	CCL4	26.63 ± 0.61	7.45 ± 1.78	0.05 ± 0.02	0.18 ± 0.01
	IL6	9.42 ± 0.46	31.45 ± 1.75	2.20 ± 0.11	0.18 ± 0.05
	IL8	4.34 ± 0.55	3.61 ± 0.96	not tested	not tested
	LTA	1.07 ± 0.22	0.73 ± 0.17	1.31 ± 0.33	2.70 ± 0.32
drug metabolism and mitochondrial function	*CYP1A2*	0.52 ± 0.05	0.48 ± 0.17	3.82 ± 0.13	13.00 ± 1.16
	UCP1	1.38 ± 0.47	0.28 ± 0.07	18.10 ± 0.19	45.49 ± 13.30
invasion and adhesion	*MMP1*	1.17 ± 0.18	1.03 ± 0.28	5.38 ± 0.40	4.51 ± 0.31
	MMP9	5.55 ± 0.31	9.85 ± 2.36	0.93 ± 0.01	1.17 ± 0.21

TABLE 3. Differences in Gene Expression for NHBE Cells Exposed to 0.5 μg/mL of 3 nm AUT-QDs or CYST-QDs for 6 h

		gene expression fold change	
associated pathway	*gene ID*	3 nm AUT-QDs (0.5 μg/mL)	3 nm CYST-QDs (0.5 μg/mL)
apoptosis and DNA damage response	*BAD*	12.03 ± 1.15	1.82 ± 0.10
	BCL-2	1.50 ± 0.24	4.28 ± 0.39
	CASP9	2.1 ± 0.35	1.35 ± 0.61
	GADD45A	4.39 ± 0.16	1.82 ± 0.05
cytokines and chemokines	*CCR3*	8.32 ± 1.31	1.46 ± 0.16
	CCR4	8.26 ± 2.16	1.92 ± 0.60
	CSF2	4.19 ± 1.25	0.25 ± 0.01
	CXCL1	3.54 ± 0.12	1.35 ± 0.09
	CXCL2	10.99 ± 0.60	0.93 ± 0.05
	CXCL3	4.55 ± 0.64	0.32 ± 0.02
	IL1α	24.62 ± 4.88	6.42 ± 1.45
	IL1β	2.05 ± 0.18	3.46 ± 0.12
	IL6	6.43 ± 1.20	0.54 ± 0.06
	VEGF	2.79 ± 0.17	1.83 ± 0.14
drug metabolism and mitochondrial function	*ARNT*	3.59 ± 0.29	1.51 ± 0.12
	CYP1A1	0.32 ± 0.11	38.28 ± 4.75
	CYP1B1	0.29 ± 0.01	47.60 ± 0.32
	UCP3	2.26 ± 0.23	2.31 ± 0.38
invasion and adhesion	*MMP9*	2.97 ± 0.30	2.10 ± 0.27
signal transduction	*JUN*	10.78 ± 0.78	0.38 ± 0.02
	MYC	4.26 ± 0.13	6.15 ± 0.30
	PIK3R1	5.25 ± 0.18	1.21 ± 0.11

produced no apoptosis at any concentrations. Furthermore, considering core size, as well, smaller positively charged CYST-QDs (3 nm) are relatively benign compared to larger positively charged QDs (5 and 10 nm). The opposite size relation is observed for negatively charged QDs. Here, 3 nm negatively charged MUA-QDs are relatively more necrotic than 5 and 10 nm MUA-QDs. Short-chain MPA-QDs induced neither necrosis nor apoptosis, irrespective of concentration (up to 160 μg/mL) and core size, while in general, MUA-QDs exhibited a cytotoxic response. Hence, while previous studies have shown that MPA- and CYST-capped CdSe QDs were cytotoxic to rat PC12 cells,[26] we did not observe any cytotoxicity with the MPA-coated QDs in human primary lung cells at the different sizes and at relatively higher concentrations. This discrepancy underscores the importance of testing the toxicity of nanomaterials in biomodels that are relevant to human exposures and are extrapolatable to human responses. It must also be noted that, even though cells were treated with the same mass concentrations for each QD size, 10 nm QD suspensions at 20 μg/mL contain between 1.5 and 2.5 orders of magnitude less

TABLE 4. Summary of Cellular Responses to QDs[a]

	long ligands						short ligands					
	MUA-QDs			AUT-QDs			MPA-QDs			CYST-QDs		
cell response	3 nm	5 nm	10 nm	3 nm	5 nm	10 nm	3 nm	5 nm	10 nm	3 nm	5 nm	10 nm
necrosis	+++	+	0	++	+++	++	0	0	0	0	+	+
apoptosis	+	++	+	+	0	0	0		0	0	+	0
proliferation	---	---	0	---	---	---	0	-	-	--	+	+
reactive oxygen species	+++	+++	+	++	+	++	0	+++	0	+	0	0

[a] The number of + corresponds to the number of concentrations that resulted a significant increase in response. The number of − corresponds to the number of concentrations that resulted in a significant decrease in response. The fields marked with 0 indicate that none of the concentrations tested resulted in a significant increase or decrease in response.

QDs than a 20 μg/mL suspension of 3 nm QDs. While this may explain the disparity between cytotoxicity for the 3 nm MUA-QDs and lack thereof for the large (10 nm) MUA-QDs, this argument is not supported for the other QDs. As such, we conclude that size (and as a direct result, particle number) is not the sole driver behind QD-induced cytotoxicity. This is further reiterated by the lack of correlation between aggregation characteristics and observed cytotoxic response. It is interesting to note that the 5 nm QDs were synthesized by adding more Cd-oleate into a solution of 3 nm CdSe QDs, so there is less selenium compared to the 3 nm CdSe QDs. Therefore, the difference in Cd/Se ratio may have modified or enhanced their ability to interact with the AUT ligand, which might potentially explain the increase in hydrodynamic diameter observed for the 5 nm AUT-QDs. Nonetheless, our observations are consistent with those seen in the literature.[29]

The interplay of QD composition, core size, ligand length, and surface charge is quite complex. That said, as we have considered only one QD composition—CdSe—and observed a range of cytotoxic responses from nontoxic to highly toxic, we tentatively conclude that QD composition is not a strongly determining factor for cytotoxicity at the levels studied, even for this "heavy-metal" (Cd) containing material. Rather, we make the following observations: (1) positively charged QDs are more toxic than negatively charged QDs; (2) of negatively charged QDs, MPA-capped QDs are essentially nontoxic even at high concentrations, indicating a possible preference for short-chain, negatively charged ligands for biomedical applications (issues of long-term stability notwithstanding); and (3) of positively charged QDs, the rapid and severe necrosis elicited by both AUT- and CYST-QDs at rather low concentrations appeared to have both QD size and dose dependencies, suggesting that capping agent alone is not the sole factor in determining cytotoxicity. It is noted, however, that ligand-specific effects may be altered by modifying the nature of the ligand, for example, reducing its lability by synthesizing tethers which are bi- or multidentate. This hypothesis is currently under investigation in our laboratory. Further, upon testing the cytotoxicity of the ligands alone, we note that they are not a significant contributing source of cell death (Supplemental Figure 2), reiterating the complex interactions at play when assessing bioeffects of nanomaterials.

As anticipated, proliferative responses correlate well with the cytotoxicity effects, wherein the more cytotoxic MUA-QDs demonstrated decrease in proliferation compared to the minimally cytotoxic MPA-QDs. We also noted a size-dependent increase in necrosis with a corresponding decrease in proliferative cells (Figure 2 and Figure 4). Since the viability of the cell population correlated with the proliferation, one can conclude that the QDs do not in themselves directly affect cellular proliferation. Nevertheless, we did observe enhanced cell growth in the 5 and 10 nm CYST-QDs at 3.5 μg/mL despite the increase in cell death at the same concentration.

To determine the role of ROS, if any, in the observed cellular responses, we evaluated changes in the intracellular ROS levels in cells in response to QD exposure. Due to the semiconducting properties of CdSe (exact band gap and valence/conduction band energy levels, and hence reductive or oxidative potential, a function of QD size),[45,46] CdSe QDs might be expected to directly cause a change in ROS levels (due to electron or hole donation). Alternatively, nanoparticles may induce cells to produce ROS as a defense mechanism. Keeping treatment levels constant and comparing size alone for the 3, 5, and 10 nm MUA-capped QDs, we note a size dependency, in that the 3 nm elicits the maximum response and the 10 nm treated cells have intracellular ROS levels similar to that of control (3 > 5 > 10 nm). This was consistent across all concentrations tested, suggesting a correlation between ROS production and cytotoxicity. Therefore, the higher the ROS response elicited, the higher the cytotoxicity, at least with regards to the MUA-capped QDs. Interestingly, though, the 5 nm MPA-capped QDs, which did not induce either necrosis or apoptosis, caused a significant increase in intracellular redox levels. In the case of the positively charged QDs, at the lower concentration

of 0.5 μg/mL, the 3 nm AUT-capped QDs that induced apoptosis caused the largest increase in ROS, followed by the 5 and 10 nm QDs (3 $\gg$ 5 >10 nm). A similar response was observed with the 5 μg/mL concentration (3 > 5 $\geq$ 10 nm); however, at the higher concentration, the 3 nm elicited no response followed by the 5 and 10 nm QDs (10 $\gg$ 5 > 3 nm). No significant ROS response was observed in the cells treated with the CYST-QDs. This was further confirmed in cells pretreated with the antioxidant NAC, while NAC inhibited QD-elicited ROS generation, it did not prevent QD-induced cytotoxicity. Thus, we conclude that the mechanism of QD cytotoxicity is independent of ROS formation. Another possible scenario for QD-induced cytotoxicity is the release of free cadmium. To address this, we performed control experiments with free Cd^{2+} ions at concentrations corresponding to the maximum available concentrations found in 0.5, 5, 20, 80, and 160 μg/mL of CdSe QDs (Supplemental Figure 3). Our results indicate that even at low concentrations, Cd^{2+} induced significant necrosis that was *not* observed in QD-treated cells. No significant apoptosis was observed at any of the doses tested. These results suggest that the differential cytotoxic responses observed in our study for the different QD sizes and surface chemistries were not solely a factor of free Cd^{2+} ion content, as Cd^{2+} ions caused very different responses compared to the QD responses.

To examine the molecular events associated with the observed cellular responses as well as to identify understated effects that are not easily observable using conventional cellular level assays, we investigated gene level responses. While Zhang *et al.*[47] investigated changes in gene expression after exposure to QDs, we employed a more targeted approach. Using 96 key genes representing molecular pathways of potential relevance, we identified genes that were either up- or down-regulated by 2-fold or greater upon treatment with QDs. Interestingly, little overlap was observed in the gene responses between the negatively and positively charged QDs, independent of ligand, reiterating the role of charge in the observed effects. In general, a nontrivial increase in mitochondrial genes (UCP1 and UCP3) was observed in the 3 nm positively charged QDs. Among many of the mitochondrial fundamental functions, the generation and detoxification of reactive oxygen species (ROS) is its most important[48] and is driven by the mitochondrial membrane potential, $\Delta\psi m$. Perturbation of mitochondrial function or $\Delta\psi m$ by external stimuli can cause subtle molecular level changes which are manifested at the cellular level.[49] Uncoupling proteins (UCP1, UCP2, and UCP3) induce proton leak in response to superoxide or lipid peroxidation and serve as attenuators of reactive oxygen species production through strong or mild uncoupling.[50] Studies have shown that UCP3 actively lowers the rate of ROS production.[51] In addition, both AUT-QDs and CYST-QDs induce an 18- and 45-fold increase in UCP1 mRNA, respectively (Table 2). Transduction of the mitochondrial proton motive force into heat instead of ATP is attributed to up-regulation of UCP1 mRNA expression.[52] Interestingly, we observe a significant decrease in ATP production in AUT-QDs at all sizes and concentrations. Although the decline in ATP production is directly proportional to the necrotic nature of AUT-QDs, it is possible that this decrease may be due to other mechanisms driven by the up-regulation of uncoupling proteins and associated functions.

While many apoptotic agents initiate apoptosis by disrupting mitochondrial function,[53] apoptotic regulation involves maintaining a fine balance between pro- and anti-apoptotic proteins.[54,55] One such pro-apoptotic gene, BAD, was found to be significantly up-regulated in 3 nm AUT-capped QDs, with a concomitant increase in caspase 9, supporting the observed cellular apoptosis elicited by 3 nm AUT at 0.5 μg/mL. Similarly, BCL-2/BCL-XL-associated death promoter acts as a negative regulator of cell survival by binding to anti-apoptotic BCL-2 family members and blocking their function, thus stimulating apoptosis.[56] Thus, the up-regulation of BCL-2 at high concentrations (20 μg/mL) of AUT-QDs may be countering the actions of pro-apoptotic factors. Further, at low concentrations of 3 nm CYST-QDs, BCL-2 was found to up-regulate, which is in accordance with the low expression levels of the pro-apoptotic genes BAD and CASP9.

The 3 nm CYST-QDs significantly up-regulated cytochrome p450 genes CYP1A1, CYP1B1 (over 40-fold), and CYP1A2 (over 10-fold) with a concomitant increase in UCP1 (45-fold). Human cytochrome p450s are major enzymes involved in the metabolism of several endogenous and exogenous chemicals.[57] These are primarily membrane-associated proteins, located either in the inner membrane of mitochondria or in the endoplasmic reticulum of cells. The cytochrome p450 family can metabolize both endogenous and exogenous chemicals, and perturbations in CYP enzyme level or activity have the potential to effect metabolism and clearance of various drugs.[58] Thus, it appears that NHBE cells react to the onslaught of QDs by up-regulating genes in the p450 family as a mechanism of detoxification.

Interestingly, there were distinct differences in the type/family of genes and the extent to which they were impacted by the different QDs. Here, the negatively charged QDs (MPA and MUA) induced a proinflammatory response. In contrast, the positively charged QDs, specifically CYST-QD, significantly up-regulated mitochondrial function genes and the cytochrome p450 detoxification enzymes, whereas the AUT QDs down-regulated CYP1A1 and CYP1B1. Further, AUT-QDs induced a proinflammatory response as observed by changes in chemokine receptors CCR1, CCR3, CCR4, and ligands (CXCL1, CXCL2, CXCL3) and cytokines (IL6, IL1α). The CCR receptors are integral membrane proteins that

specifically bind and respond to cytokines of the CC chemokine family, which play an important role in the recruitment of responding immune cells, including macrophages.[59] Collectively, the gene expression results indicate that positively charged CYST-QDs might be affecting mitochondrial membrane potential by up-regulating genes associated with the mitochondria, while negatively charged MPA and MUA-QDs and also positively charged AUT-QDs may impact inflammatory pathways.

CONCLUSIONS

Through the systematic analyses of QD parameters that specifically focused on size, charge, and functionalization, we conclude that while positively charged QDs are more cytotoxic than negative QDs, longer ligands resulted in greater cytotoxicity than short ligands, independent of charge. We also posit that QD-induced mitochondrial damage might be the underlying mechanism of charge-based toxicity.

MATERIALS AND METHODS

Quantum Dot Preparation and Characterization. *Nanocrystal Synthesis.* Materials: Cadmium oxide (CdO, 99.95%) and oleic acid (90%) were purchased from Alfa Aesar, 1-octadecene (ODE, 90%) from Acros Organics, oleylamine (tech grade) and selenium pellet (≥99.999%) from Aldrich, trioctylphosphine (TOP, 97%) and trioctylphosphine oxide (TOPO, 90%) from Strem. All chemicals were used without any further purification.

Synthesis of precursors: Cadmium oleate was synthesized by heating 1.45 g of CdO in 20 mL of oleic acid at 170 °C until the solution becomes colorless. It was then allowed to cool to 100 °C, at which point it was degassed under vacuum. TOP-Se was prepared in an inert atmosphere glovebox by dissolving 3.95 g of Se pellet in 50 mL of TOP.

CdSe QDs: Using standard air-free handling methods, a 100 mL round-bottom flask was loaded with 1 g of TOPO, 8 mL of ODE, and 0.75 mL of cadmium oleate. The reaction mixture was thoroughly degassed at room temperature, as well as at 80 °C, before raising the temperature to 300 °C under an atmosphere of UHP argon. A mixture of 4 mL of TOP-Se, 3 mL of oleylamine, and 1 mL of ODE was then quickly injected into the reaction system. The temperature was subsequently lowered to 270 °C for CdSe QD growth.[60] After ~1 min, the solution was allowed to cool, yielding CdSe QDs with a diameter of 3 nm. Larger CdSe QDs (5 nm) were synthesized by injecting a second portion of Cd-oleate (0.75 mL) at 270 °C, followed by growth for about an hour. To achieve even larger diameters, 10 times the amount of both precursors were added dropwise from an addition funnel at 240 °C to nominally 3 nm starting "core" CdSe QDs. CdSe QDs were collected by precipitation with acetone followed by centrifugation. A second purification step was done with methanol precipitation. The CdSe QDs were redispersible in hexane or toluene.

Ligand Exchange. Materials: Mercaptopropionic acid (MPA), mercaptoundecanoic acid (MUA), aminoundecanethiol (AUT), and cysteamine (CYST) and tetramethylammonium hydroxide (TMAH) were purchased from Aldrich, Fluka, Dojindo, and Acros Organics, respectively, and used without further purification.

Ligand exchange: Prior to ligand exchange, semiconductor nanocrystals were purified as indicated above to remove excess ligands from the chemical synthesis. QD concentrations were calculated according to Yu *et al.*[61] on the basis of UV−vis spectra. For the carboxyl-terminated ligands, an amount of ligand (MUA or MPA) equivalent to 2 times the moles of CdSe in the sample was added to the toluene solution. After 2 h, a solution of TMAH in water (4 times the moles of CdSe) was added dropwise. The nanocrystals transferred from the toluene phase to the water phase, as indicated by the toluene phase losing color and the water phase becoming yellow, orange, or red (depending on the size of the QD being transferred). The water phase was separated from the toluene phase and precipitated with isopropyl alcohol, followed by centrifugation (~5 min at 5000 rpm). Finally, the pellet was redispersed in distilled water. The procedure for exchange with CYST was executed in a similar fashion except that a 20-fold excess of CYST was used, and the base was replaced by acid to promote transfer into the aqueous layer. Once the QDs transferred, the pH of the solution was brought back to ~6. For exchanging ligands with AUT, the QDs were not redispersed in toluene. Rather, an emulsion of AUT in water was added to the pellet followed by extensive sonication of the sample (about 3 h). Aggregates were carefully removed by centrifugation.

Quantum Dot Characterization. As-synthesized CdSe QDs were characterized by UV−vis spectroscopy and imaged by transmission electron microscopy (TEM). Using the known correlation between optical absorption onset and particle size and concentration for CdSe QDs, diameters, as well as concentrations, were calculated by applying the relevant formulas described previously.[61] Additionally, QD diameters were confirmed by directly measuring particle sizes in TEM images, where in each case approximately 100 structures were analyzed. Neither UV−vis calculations nor TEM imaging accounts for the ligand's contribution to particle size, nor do these methods assess the QD hydrodynamic radius. Particle size in solution was determined using dynamic light scattering (DLS) methods with the hydrodynamic diameters calculated using the number distribution.

After ligand exchange and transfer to water, the concentration of CdSe QDs was again calculated using literature formulas.[61] Furthermore, DLS and zeta-potential measurements were performed using a Malvern zetasizer to determine the hydrodynamic diameter, as well as surface charge. From these measurements, we were able to estimate the degree of monodispersity and stability of the nanoparticles in aqueous solution.

Biological Methods. *Cell Culture and Exposure.* Normal human bronchial epithelial (NHBE) cells were purchased (Lonza, Walkersville, MD) and cultured using bronchial epithelial cell growth media (BEGM, Clonetics Bullet Kit Lonza, Walkersville, MD) on 100 mm tissue culture treated Petri dishes (Santa Cruz Biotechnologies, Santa Cruz, CA) coated with 50 μg/mL type I rat tail collagen (BD Biosciences, Bedford, MA). Cells were stored in a 37 °C incubator with a humidified atmosphere at 5% CO_2. Cells were fed two times weekly and passaged *via* trypsinization. Experimentation was performed in triplicate on cells harvested from passages 3 to 7.

NHBE cells were plated in 96-well tissue culture plates at a concentration of 1.5×10^4 cells/well in a volume of 200 μL and allowed to acclimate overnight. Prior to exposure to QDs suspended at 20, 80, or 160 μg/mL (negative QDs) or 0.5, 5, or 20 μg/mL (positive QDs) in either phenol-red free Hanks balanced salt solution (HBSS) for reactive oxygen species (ROS) experiments or BEGM. A conversion to molar concentrations and particle numbers for each treatment can be found in Supplemental Table 3. During the exposure period, plates were maintained in a humidified incubator at 37 °C and 5% CO_2.

Proliferation and Cytotoxicity Assay. After 24 h of exposure, plates were centrifuged at 200*g* for 5 min and 75 μL of supernatant was taken from each well and transferred to a new flat bottom plate for later analyses of lactate dehydrogenase (LDH) activity. Plates were covered and stored at 4 °C until analysis was performed.

To assess cellular proliferation, water-soluble tetrazolium (WST-1) reagent (Clontech, Mountain View, CA) was used according to the manufacturers' instructions. NHBE cells exposed to media only and 1% Triton in BEGM were included as controls. QD controls at the highest concentrations tested were included in wells without cells to determine if QDs interfere with WST-1 reagent.

The amount of LDH in supernatants can be measured and used as an indirect measure of cell membrane permeability. Thus, the cytotoxic effects of QD exposure on NHBE cells was evaluated by measuring LDH activity using a LDH cytoxicity kit (Clontech, Mountain View, CA) as outlined in Martin *et al.*[62] NHBE cells exposed to media only or 1% Triton-100 in BEGM served as controls. QD controls at the highest concentrations tested were included in wells without cells to determine if QDs interfere with LDH reaction mix.

Oxidative Stress. Reactive Oxygen Species Measurements. Intracellular ROS in NHBE cells exposed to QDs were measured using 5-(and-6)-carboxy-2′,7′-dichlorodihydrofluorescein diacetate, acetyl ester (CM-H_2DCFDA), purchased from Molecular Probes, Invitrogen, Eugene, OR, as previously described.[62] NHBE cells exposed to HBSS only or 100 μM H_2O_2 served as controls. QD controls at the highest concentrations were included in wells without cells to determine if QDs induce spontaneous fluorescence of CM-H_2DCFDA.

NAC Treatment. Cells were washed and incubated with HBSS for 15 min, then treated with a 5 μM solution of CM-H_2DCFDA for 30 min. Cells were then washed with HBSS and pretreated with *n*-acetyl cysteine (NAC, Sigma Aldrich) at a concentration of 5 mM prepared in HBSS for 30 min. HBSS was aspirated, and NHBE cells were exposed to QDs suspended in HBSS containing 5 mM NAC for 60 min prior to reading using an excitation wavelength of 490 nm and emission wavelength of 535 nm.

Apoptosis. A hallmark of apoptosis is the cleavage of DNA *via* endogenous endonuclease, which results in the presence of 180 bp DNA fragments. To determine if QD exposure induces apoptosis in NHBE cells, levels of mono- and oligonucleosomes in cell lysates were measured using cell death detection ELISA kits (Roche Applied Science, Germany) as outlined in Gao *et al.*[62]

Acridine Orange/Ethidium Bromide Staining (AO/EB). Cells were dual stained with acridine orange and ethidium iodide as previously described,[62] which can be used to microscopically identify events in cells consistent with apoptosis, such as the appearance of apoptotic bodies and nuclear changes. Stained cells were immediately analyzed using a fluorescence microscope with 10× objective (Zeiss Axiophot, Carl Zeiss, Germany) and imaged using Pro Plus software (version 6.2, Media Cybernetics, Silver Spring, MD). NHBE cells exposed to media only, 1% Triton-100 in media, or 12 μM camptothecin served as controls. Apoptotic cells were delineated with orange nuclei, and live cells appear uniformly green.

To determine if antioxidants could preserve cellular viability, NHBE cells were incubated with QDs suspended in media containing 5 mM NAC over a period of 24 h. Cells were washed two times with DPBS prior to staining with AO/EB as stated above.

Gene Expression Analyses. Differences in gene expression were assessed using the BioMark real-time PCR high-throughput chip system and 96.96 dynamic arrays (Fluidigm, CA). The 96 TaqMan assays selected for this study are representative of cellular pathways associated with apoptosis, mitochondrial function, oxidative stress, cell cycle arrest, inflammation, and extracellular matrix formation; a complete list of genes tested and their associated pathways can be found in Supplemental Table 3. NHBE cells were exposed to QDs for 6 h prior to RNA purification using RNeasy Mini-Kit (Qiagen, CA) according to manufacturer's instructions. RNA quality was assessed and quantified using the Agilent 2100 BioAnalyzer RNA Nano chip system (Agilent Technologies, CA) prior to further manipulation. First strand cDNA synthesis from 1 μg of RNA was performed using a high-capacity cDNA reverse transcription kit according to manufacturer's instructions (Life Technologies (Applied Biosystems), CA). To enable expression studies across 96 assays, cDNA was subjected to preamplification. For preamplification of cDNA, 96 TaqMan assays were pooled to a final concentration of 0.2× for each assay. Preamplification PCR reactions were performed in a total volume of 10 μL, each containing 5 μL TaqMan PreAmp master mix (2×), 2.5 μL of pooled TaqMan assay mix (0.2×), and 2.5 μL (125 ng) of cDNA. The preamplification PCR was performed as follows: one cycle at 95 °C for 10 min, 14 cycles at 95 °C for 15 s, and then at 60 °C for 4 min. After preamplification PCR, the product was diluted 1:5 with TE buffer and stored at −20 °C until real-time PCR analyses could be performed.

For the real-time PCR analyses, a sample premix consisting of 3.5 μL of 2× TaqMan fast universal master mix (Life Technologies (Applied Biosystems), CA) and 0.35 μL of 20× GE sample loading reagent (Fluidigm, CA) per sample was prepared; 3.5 μL of the sample premix was aliquoted into individual wells of a 96-well PCR plate. To the plate containing sample premix was added 3.15 μL of preamped sample cDNA to each well; the plate was then vortexed, centrifuged, and placed on ice until the chip was ready to load. TaqMan gene expression assays were prepared in a separate individual 96-well PCR plate; each well contained 3 μL of a single 20× assay and 3 μL of 2× assay loading reagent (Fluidigm, CA).

The 96.96 dynamic array chips were primed using the preset protocol on the IFC Controller HX. The chip inlets were then loaded accordingly with 5 μL of sample per inlet and 5 μL of TaqMan assay per inlet, and the chip was processed and loaded using the IFC Controller HX. After loading the chip, real-time PCR was performed on the BioMark instrument using BioMark HD data collection software v3.0.2.

Real-time PCR analyses were performed using Fluidigm real-time PCR analysis software. Sample ΔC_t values were calculated by using a negative control (media only). $\Delta\Delta C_t$ values were calculated for the TaqMan assays using β-actin as the normalizer reference gene. An 18S rRNA TaqMan assay served as an endogenous control. Significant changes in gene expression are reported as those genes whose expression was increased greater than 2-fold.

Statistical Analyses. Significant differences between treatments were determined using one-way analysis of variance (ANOVA) with pairwise comparisons using Tukey's test. Analyses were performed using SigmaPlot version 11.0 (Systat Software, Inc., San Jose, CA). Experiments were performed a minimum of three independent times with cells on different passage numbers. When necessary, data were transformed using log or square root transformations to conform to normality and equal variance. Significance was determined when $p < 0.05$, and graph values are represented by mean ± standard deviation.

Conflict of Interest: The authors declare no competing financial interest.

Acknowledgment. This work was supported by Los Alamos National Laboratory LDRD-DR program. This work was performed, in part, at the Center for Integrated Nanotechnologies, a U.S. Department of Energy, Office of Basic Energy Sciences user facility. Los Alamos National Laboratory, an affirmative action equal opportunity employer, is operated by Los Alamos National Security, LLC, for the National Nuclear Security Administration of the U.S. Department of Energy under contract DE-AC52-06NA25396. We also thank Priya Dighe and Melinda Henrie for their expertise and help using the BioMark Fluidigm systems. The technical assistance of Jonathan Thoma was greatly appreciated.

Supporting Information Available: Supplemental methods for cadmium ion exposure to NHBE cells are available. Supplemental TEM data are available in Supplemental Table 1. Conversions of mass concentration to molar and particle concentrations are listed in Supplemental Table 2. A comprehensive list of genes studied for changes in gene expression and their associated cellular response pathways can be found in Supplemental Table 3. Supplemental Figure 1 details the necrosis of 3 nm CYST-QDs at 80 and 160 μg/mL. Supplemental Figure 2 illustrates the cytotoxicity induced on NHBE cells by ligands alone. Supplemental Figure 3 shows viability data of NHBE cells exposed to cadmium ion concentrations equivalent to the amount of cadmium contained in QDs by mass/volume.

This material is available free of charge *via* the Internet at http://pubs.acs.org.

REFERENCES AND NOTES

1. Chen, Y.; Vela, J.; Htoon, H.; Casson, J. L.; Werder, D. J.; Bussian, D. A.; Klimov, V. I.; Hollingsworth, J. A. "Giant" Multishell CdSe Nanocrystal Quantum Dots with Suppressed Blinking. *J. Am. Chem. Soc.* **2008**, *130*, 5026–5027.
2. Mahler, B.; Spinicelli, P.; Buil, S.; Quelin, X.; Hermier, J. P.; Dubertret, B. Towards Non-blinking Colloidal Quantum Dots. *Nat. Mater.* **2008**, *7*, 659–664.
3. Vela, J.; Htoon, H.; Chen, Y.; Park, Y. S.; Ghosh, Y.; Goodwin, P. M.; Werner, J. H.; Wells, N. P.; Casson, J. L.; Hollingsworth, J. A. Effect of Shell Thickness and Composition on Blinking Suppression and the Blinking Mechanism in `Giant' CdSe/CdS Nanocrystal Quantum Dots. *J. Biophotonics* **2010**, *3*, 706–717.
4. Wang, X.; Ren, X.; Kahen, K.; Hahn, M. A.; Rajeswaran, M.; Maccagnano-Zacher, S.; Silcox, J.; Cragg, G. E.; Efros, A. L.; Krauss, T. D. Non-blinking Semiconductor Nanocrystals. *Nature* **2009**, *459*, 686–689.
5. Hu, M.; Yan, J.; He, Y.; Lu, H.; Weng, L.; Song, S.; Fan, C.; Wang, L. Ultrasensitive, Multiplexed Detection of Cancer Biomarkers Directly in Serum by Using a Quantum Dot-Based Microfluidic Protein Chip. *ACS Nano* **2010**, *4*, 488–494.
6. Liandris, E.; Gazouli, M.; Andreadou, M.; Sechi, L. A.; Rosu, V.; Ikonomopoulos, J. Detection of Pathogenic Mycobacteria Based on Functionalized Quantum Dots Coupled with Immunomagnetic Separation. *PLoS ONE* **2011**, *6*, e20026.
7. Sanvicens, N.; Pascual, N.; Fernández-Argüelles, M.; Adrián, J.; Costa-Fernández, J.; Sánchez-Baeza, F.; Sanz-Medel, A.; Marco, M. P. Quantum Dot-Based Array for Sensitive Detection of *Escherichia coli*. *Anal. Bioanal. Chem.* **2011**, *399*, 2755–2762.
8. Tripp, R. A.; Alvarez, R.; Anderson, B.; Jones, L.; Weeks, C.; Chen, W. Bioconjugated Nanoparticle Detection of Respiratory Syncytial Virus Infection. *Int. J. Nanomed.* **2007**, *2*, 117–124.
9. Courty, S.; Bouzigues, C.; Luccardini, C.; Ehrensperger, M. V.; Bonneau, S.; Dahan, M. Tracking Individual Proteins in Living Cells Using Single Quantum Dot Imaging. *Methods Enzymol.* **2006**, *414*, 211–228.
10. Garon, E. B.; Marcu, L.; Luong, Q.; Tcherniantchouk, O.; Crooks, G. M.; Koeffler, H. P. Quantum Dot Labeling and Tracking of Human Leukemic, Bone Marrow and Cord Blood Cells. *Leuk. Res.* **2007**, *31*, 643–651.
11. Iyer, G.; Michalet, X.; Chang, Y. P.; Weiss, S. Tracking Single Proteins in Live Cells Using Single-Chain Antibody Fragment-Fluorescent Quantum Dot Affinity Pair. *Methods Enzymol.* **2010**, *475*, 61–79.
12. Joo, K. I.; Lei, Y.; Lee, C. L.; Lo, J.; Xie, J.; Hamm-Alvarez, S. F.; Wang, P. Site-Specific Labeling of Enveloped Viruses with Quantum Dots for Single Virus Tracking. *ACS Nano* **2008**, *2*, 1553–1562.
13. Roullier, V.; Clarke, S.; You, C.; Pinaud, F.; Gouzer, G. R.; Schaible, D.; Marchi-Artzner, V. R.; Piehler, J.; Dahan, M. High-Affinity Labeling and Tracking of Individual Histidine-Tagged Proteins in Live Cells Using Ni^{2+} Tris-Nitrilotriacetic Acid Quantum Dot Conjugates. *Nano Lett.* **2009**, *9*, 1228–1234.
14. Yum, K.; Na, S.; Xiang, Y.; Wang, N.; Yu, M. F. Mechanochemical Delivery and Dynamic Tracking of Fluorescent Quantum Dots in the Cytoplasm and Nucleus of Living Cells. *Nano Lett.* **2009**, *9*, 2193–2198.
15. Clapp, A. R.; Medintz, I. L.; Uyeda, H. T.; Fisher, B. R.; Goldman, E. R.; Bawendi, M. G.; Mattoussi, H. Quantum Dot-Based Multiplexed Fluorescence Resonance Energy Transfer. *J. Am. Chem. Soc.* **2005**, *127*, 18212–18221.
16. Crut, A.; Géron-Landre, B.; Bonnet, I.; Bonneau, S.; Desbiolles, P.; Escudé, C. Detection of Single DNA Molecules by Multicolor Quantum-Dot End-Labeling. *Nucleic Acids Res.* **2005**, *33*, e98.
17. Geho, D. H.; Killian, J. K.; Nandi, A.; Pastor, J.; Gurnani, P.; Rosenblatt, K. P. Fluorescence-Based Analysis of Cellular Protein Lysate Arrays Using Quantum Dots. *Methods Mol. Biol.* **2007**, *374*, 229–237.
18. Ohyanagi, T.; Nagahori, N.; Shimawaki, K.; Hinou, H.; Yamashita, T.; Sasaki, A.; Jin, T.; Iwanaga, T.; Kinjo, M.; Nishimura, S. I. Importance of Sialic Acid Residues Illuminated by Live Animal Imaging Using Phosphorylcholine Self-Assembled Monolayer-Coated Quantum Dots. *J. Am. Chem. Soc.* **2011**, *133*, 12507–12517.
19. Zhang, G.; Shi, L.; Selke, M.; Wang, X. CdTe Quantum Dots with Daunorubicin Induce Apoptosis of Multidrug-Resistant Human Hepatoma HepG2/ADM Cells: *In Vitro* and *In Vivo* Evaluation. *Nanoscale Res. Lett* **2011**, *6*, 418–428.
20. Zintchenko, A.; Susha, A. S.; Concia, M.; Feldmann, J.; Wagner, E.; Rogach, A. L.; Ogris, M. Drug Nanocarriers Labeled with Near-Infrared-Emitting Quantum Dots (Quantoplexes): Imaging Fast Dynamics of Distribution in Living Animals. *Mol. Ther.* **2009**, *17*, 1849–1856.
21. Bagalkot, V.; Zhang, L.; Levy-Nissenbaum, E.; Jon, S.; Kantoff, P. W.; Langer, R.; Farokhzad, O. C. Quantum Dot−Aptamer Conjugates for Synchronous Cancer Imaging, Therapy, and Sensing of Drug Delivery Based on Bi-Fluorescence Resonance Energy Transfer. *Nano Lett.* **2007**, *7*, 3065–3070.
22. Lim, Y. T.; Cho, M. Y.; Noh, Y. W.; Chung, J. W.; Chung, B. H. Near-Infrared Emitting Fluorescent Nanocrystals-Labeled Natural Killer Cells as a Platform Technology for the Optical Imaging of Immunotherapeutic Cells-Based Cancer Therapy. *Nanotechnology* **2009**, *20*, 475102.
23. Cho, S. J.; Maysinger, D.; Jain, M.; Röder, B.; Hackbarth, S.; Winnik, F. M. Long-Term Exposure to CdTe Quantum Dots Causes Functional Impairments in Live Cells. *Langmuir* **2007**, *23*, 1974–1980.
24. Li, H.; Li, M.; Shih, W. Y.; Lelkes, P. I.; Shih, W. H. Cytotoxicity Tests of Water Soluble ZnS and CdS Quantum Dots. *J. Nanosci. Nanotechnol.* **2011**, *11*, 3543–3551.
25. Wang, L.; Nagesha, D.; Selvarasah, S.; Dokmeci, M.; Carrier, R. Toxicity of CdSe Nanoparticles in Caco-2 Cell Cultures. *J. Nanobiotechnol.* **2008**, *6*, 11–26.
26. Lovrić, J.; Bazzi, H. S.; Cuie, Y.; Fortin, G. R.; Winnik, F. M.; Maysinger, D. Differences in Subcellular Distribution and Toxicity of Green and Red Emitting CdTe Quantum Dots. *J. Mol. Med.* **2005**, *83*, 377–385.
27. Yacobi, N. R.; Phuleria, H. C.; Demaio, L.; Liang, C. H.; Peng, C. A.; Sioutas, C.; Borok, Z.; Kim, K. J.; Crandall, E. D. Nanoparticle Effects on Rat Alveolar Epithelial Cell Monolayer Barrier Properties. *Toxicol. in Vitro* **2007**, *21*, 1373–1381.
28. Nagy, A.; Zane, A.; Cole, S. L.; Severance, M.; Dutta, P. K.; Waldman, W. J. Contrast of the Biological Activity of Negatively and Positively Charged Microwave Synthesized CdSe/ZnS Quantum Dots. *Chem. Res. Toxicol.* **2011**, *24*, 2176–2188.
29. Hoshino, A.; Fujioka, K.; Oku, T.; Suga, M.; Sasaki, Y. F.; Ohta, T.; Yasuhara, M.; Suzuki, K.; Yamamoto, K. Physicochemical Properties and Cellular Toxicity of Nanocrystal Quantum Dots Depend on Their Surface Modification. *Nano Lett.* **2004**, *4*, 2163–2169.
30. Hoshino, A.; Hanada, S.; Yamamoto, K. Toxicity of Nanocrystal Quantum Dots: The Relevance of Surface Modifications. *Arch. Toxicol.* **2011**, *85*, 707–720.
31. Clift, M. J.; Rothen-Rutishauser, B.; Brown, D. M.; Duffin, R.; Donaldson, K.; Proudfoot, L.; Guy, K.; Stone, V. The Impact of Different Nanoparticle Surface Chemistry and Size on Uptake and Toxicity in a Murine Macrophage Cell Line. *Toxicol. Appl. Pharmacol.* **2008**, *232*, 418–427.
32. Ryman-Rasmussen, J. P.; Riviere, J. E.; Monteiro-Riviere, N. A. Surface Coatings Determine Cytotoxicity and Irritation Potential of Quantum Dot Nanoparticles in Epidermal Keratinocytes. *J. Invest. Dermatol.* **2007**, *127*, 143–153.
33. Tang, M.; Wang, M.; Xing, T.; Zeng, J.; Wang, H.; Ruan, D. Y. Mechanisms of Unmodified CdSe Quantum Dot-Induced Elevation of Cytoplasmic Calcium Levels in Primary Cultures of Rat Hippocampal Neurons. *Biomaterials* **2008**, *29*, 4383–4391.

34. Kuo, T. R.; Lee, C. F.; Lin, S. J.; Dong, C. Y.; Chen, C. C.; Tan, H. Y. Studies of Intracorneal Distribution and Cytotoxicity of Quantum Dots: Risk Assessment of Eye Exposure. *Chem. Res. Toxicol.* **2011**, *24*, 253–261.
35. Malvern. Zeta Potential: An Introduction in 30 minutes, **2011**.
36. Martelli, A.; Rousselet, E.; Dycke, C.; Bouron, A.; Moulis, J. M. Cadmium Toxicity in Animal Cells by Interference with Essential Metals. *Biochimie* **2006**, *88*, 1807–1814.
37. Moulis, J. M. Cellular Mechanisms of Cadmium Toxicity Related to the Homeostasis of Essential Metals. *BioMetals* **2010**, *23*, 877–896.
38. Nogueira, C.; Rocha, J. Toxicology and Pharmacology of Selenium: Emphasis on Synthetic Organoselenium Compounds. *Arch. Toxicol.* **2011**, *85*, 1313–1359.
39. Nogueira, C. W.; Zeni, G.; Rocha, J. B. T. Organoselenium and Organotellurium Compounds: Toxicology and Pharmacology. *Chem. Rev.* **2004**, *104*, 6255–6286.
40. Nordberg, G. F. Historical Perspectives on Cadmium Toxicology. *Toxicol. Appl. Pharmacol.* **2009**, *238*, 192–200.
41. Taylor, A. Biochemistry of Tellurium. *Biol. Trace Elem. Res.* **1996**, *55*, 231–239.
42. Tinggi, U. Essentiality and Toxicity of Selenium and its Status in Australia: A Review. *Toxicol. Lett.* **2003**, *137*, 103–110.
43. Su, Y.; He, Y.; Lu, H.; Sai, L.; Li, Q.; Li, W.; Wang, L.; Shen, P.; Huang, Q.; Fan, C. The Cytotoxicity of Cadmium Based, Aqueous Phase - Synthesized, Quantum Dots and Its Modulation by Surface Coating. *Biomaterials* **2009**, *30*, 19–25.
44. Zhang, Y.; Chen, Y.; Westerhoff, P.; Crittenden, J. C. Stability and Removal of Water Soluble CdTe Quantum Dots in Water. *Environ. Sci. Technol.* **2007**, *42*, 321–325.
45. Ekimov, A. I.; Onushchenko, A. A. Quantum Size Effect in Three-Dimensional Microscopic Semiconductor Crystals. *J. Exp. Theor. Phys. Lett.* **1981**, *34*, 363–366.
46. Ekimov, A. I.; Onushchenko, A. A. Size Quantization of the Electron Energy Spectrum in a Microscopic Semiconductor Crystal. *J. Exp. Theor. Phys. Lett.* **1984**, *40*, 337–340.
47. Zhang, T.; Stilwell, J. L.; Gerion, D.; Ding, L.; Elboudwarej, O.; Cooke, P. A.; Gray, J. W.; Alivisatos, A. P.; Chen, F. F. Cellular Effect of High Doses of Silica-Coated Quantum Dot Profiled with High Throughput Gene Expression Analysis and High Content Cellomics Measurements. *Nano Lett.* **2006**, *6*, 800–808.
48. Turrens, J. F. Mitochondrial Formation of Reactive Oxygen Species. *J. Physiol.* **2003**, *552*, 335–344.
49. Wright, D. T.; Cohn, L. A.; Li, H.; Fischer, B.; Li, C. M.; Adler, K. B. Interactions of Oxygen Radicals with Airway Epithelium. *Environ. Health Perspect.* **1994**, *102*, 85–90.
50. Azzu, V.; Jastroch, M.; Divakaruni, A. S.; Brand, M. D. The Regulation and Turnover of Mitochondrial Uncoupling Proteins. *Biochim. Biophys. Acta* **2010**, *1797*, 785–791.
51. Toime, L. J.; Brand, M. D. Uncoupling Protein-3 Lowers Reactive Oxygen Species Production in Isolated Mitochondria. *Free Radical Biol. Med.* **2010**, *49*, 606–611.
52. Nicholls, D. G.; Locke, R. M. Thermogenic Mechanisms in Brown Fat. *Physiol. Rev.* **1984**, *64*, 1–64.
53. Gupta, S.; Kass, G. E.; Szegezdi, E.; Joseph, B. The Mitochondrial Death Pathway: A Promising Therapeutic Target in Diseases. *J. Cell. Mol. Med.* **2009**, *13*, 1004–1033.
54. Green, D. R. Apoptotic Pathways: Ten Minutes to Dead. *Cell (Cambridge)* **2005**, *121*, 671–674.
55. Green, D. R.; Reed, J. C. Mitochondria and Apoptosis. *Science* **1998**, *281*, 1309–1312.
56. Youle, R. J.; Strasser, A. The BCL-2 Protein Family: Opposing Activities That Mediate Cell Death. *Nat. Rev. Mol. Cell Biol.* **2008**, *9*, 47–59.
57. Nebert, D. W.; Dalton, T. P. The Role of Cytochrome P450 Enzymes in Endogenous Signalling Pathways and Environmental Carcinogenesis. *Nat. Rev. Cancer* **2006**, *6*, 947–960.
58. Guengerich, F. P. Cytochrome P450 and Chemical Toxicology. *Chem. Res. Toxicol.* **2007**, *21*, 70–83.
59. Mahler, B.; Lequeux, N.; Dubertret, B. T. Ligand-Controlled Polytypism of Thick-Shell CdSe/CdS Nanocrystals. *J. Am. Chem. Soc.* **2009**, *132*, 953–959.
60. Yu, W. W.; Qu, L.; Guo, W.; Peng, X. Experimental Determination of the Extinction Coefficient of CdTe, CdSe, and CdS Nanocrystals. *Chem. Mater.* **2003**, *15*, 2854–2860.
61. Martin, R.; Wang, H. L.; Gao, J.; Iyer, S.; Montaño, G. A.; Martinez, J.; Shreve, A. P.; Bao, Y.; Wang, C. C.; Chang, Z.; *et al.* Impact of Physicochemical Properties of Engineered Fullerenes on Key Biological Responses. *Toxicol. Appl. Pharmacol.* **2009**, *234*, 58–67.
62. Gao, J.; Wang, H. L.; Shreve, A.; Iyer, R. Fullerene Derivatives Induce Premature Senescence: A New Toxicity Paradigm or Novel Biomedical Applications. *Toxicol. Appl. Pharmacol.* **2010**, *244*, 130–143.